HHS Public Access

Author manuscript

Mater Sci Eng C Mater Biol Appl. Author manuscript; available in PMC 2022 June 01.

Published in final edited form as:

Mater Sci Eng C Mater Biol Appl. 2021 June ; 125: 112100. doi:10.1016/j.msec.2021.112100.

Fabrication of PNIPAm-based Thermoresponsive Hydrogel Microwell Arrays for Tumor Spheroid Formation

Dinesh Dhamecha[1], **Duong Le**[1], **Tomali Chakravarty**[2], **Kalindu Perera**[1], **Arnob Dutta**[2], **Jyothi U. Menon**[1,*]

[1]Department of Biomedical and Pharmaceutical Sciences, College of Pharmacy, University of Rhode Island, Kingston, RI 02881, USA

[2]Department of Cell and Molecular Biology, College of Environment and Life Sciences, University of Rhode Island, Kingston, RI 02881, USA

Abstract

Complex three-dimensional (3D) cell cultures are being increasingly implemented in biomedical research as they provide important insights into complex cancer biology, and cell-cell and cell-matrix interactions in the tumor microenvironment. However, most methods used today for 3D cell culture are limited by high cost, the need for specialized skills, low throughput and the use of unnatural culture environments. We report the development of a unique biomimetic hydrogel microwell array platform for the generation and stress-free isolation of cancer spheroids. The poly N-isopropylacrylamide-based hydrogel microwell array (PHMA) has thermoresponsive properties allowing for the attachment and growth of cell aggregates/ spheroids at 37°C, and their easy isolation at room temperature (RT). The reversible phase transition of the microwell arrays at 35°C was confirmed visually and by differential scanning calorimetry. Swelling/ shrinking studies and EVOS imaging established that the microwell arrays are hydrophilic and swollen at temperatures <35°C, while they shrink and are hydrophobic at temperatures >35°C. Spheroid development within the PHMA was optimized for seeding density, incubation time and cell viability. Spheroids of A549, HeLa and MG-63 cancer cell lines, and human lung fibroblast (HLF) cell line generated

[*]**Corresponding Author**: Dr. Jyothi U. Menon, Assistant Professor, Department of Biomedical and Pharmaceutical Sciences, University of Rhode Island, 7 Greenhouse Road, Kingston, RI 02881, Telephone : (401) 874-4914. jmenon@uri.edu.

Author Contributions

The manuscript was written through contributions of all authors. All authors have given approval to the final version of the manuscript. DD contributed in designing and conducting all experiments, data analysis, writing, reviewing and editing manuscript. DL, KP, AD, and TC contributed by performing hypoxia experiment, confocal microscopy, analysis; image processing and analysis; reviewing and editing manuscript. JM contributed by conceptualizing, mentoring, fund acquisition, reviewing and was responsible for final editing of manuscript.

Declaration of competing interest

The authors report no conflicts of interest in this work.

Declaration of interests

The authors declare that they have no known competing financial interests or personal relationships that could have appeared to influence the work reported in this paper.

Supporting information

File consists of results from mechanical testing of the hydrogel and HepG2 cell spheroid formation using the PHMA.

within the PHMAs had relatively spherical morphology with hypoxic cores. Finally, using MG-63 cell spheroids as representative models, a proof-of-concept drug response study using doxorubicin hydrochloride was conducted. Overall, we demonstrate that the PHMAs are an innovative alternative to currently used 3D cell culture techniques, for the high-throughput generation of cell spheroids for disease modeling and drug screening applications.

Graphical abstract

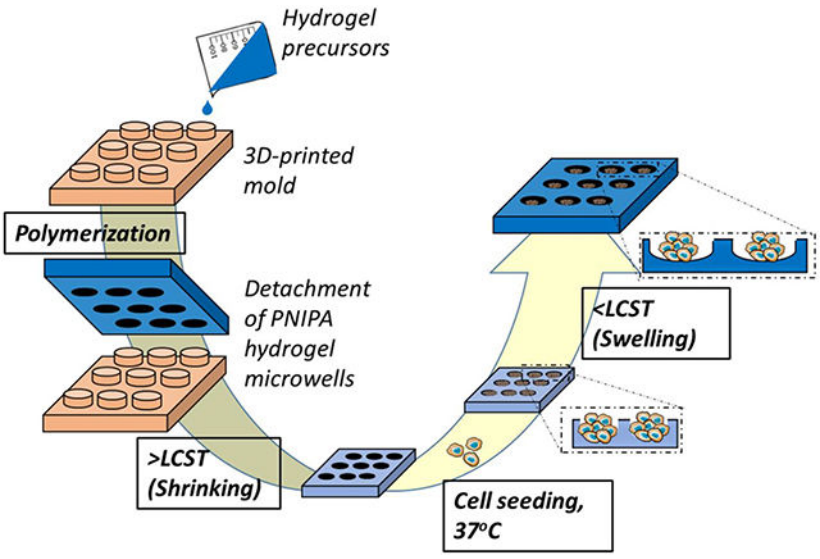

Keywords

PNIPAm; microwell array; hydrogel; spheroids; biomimetic; thermoresponsive

1. INTRODUCTION

Cancer drug discovery is an expensive process as large capital investments (average estimate = $2.87 billion) are required to take a drug from synthesis to clinical trials, and into the market [1]. Despite the high development costs, most drugs that show promise during preclinical investigation tend to fail during clinical trials. This could be attributed, in part, to the use of two-dimensional (2D) cell culture models for early drug testing, although these models do not fully recapitulate clinical cancer condition [2-4]. Therefore, there is an urgent need to develop specialized *in vitro* cell culture models that more closely mimic cellular arrangements and interactions observed in an *in vivo* environment. These models are expected to provide more predictive responses to the tested therapeutics than 2D cell culture systems.

Complex three-dimensional (3D) cell cultures are being increasingly used in biomedical research as they provide important insights into understanding cancer biology, and cell-cell interactions in the tumor microenvironment [5-8]. Some of the commonly used methods for the development of complex *in vitro* tumor models are hanging drop [9-11], spinner flasks [12,13], nonadherent plates/dishes [14,15] and microfluidics platforms [16-18]. However,

the hanging drop method is limited by difficulty in changing media and low-throughput spheroid generation, the spinner flask by long incubation times, and microfluidics methods by the need for specialized instrumentation and skills [16]. Nonadherent plates/ dishes are most commonly used for spheroid generation [14], however these platforms utilize an unnatural low-attachment environment in which the cells are forced to remain suspended and aggregate to form spheroids. However, cells within the body are not found in a suspended state; instead, they tend to bind to and grow on the extracellular matrices (ECM) [19,20]. Hence, there is a need for methodologies that more closely mimic *in vivo* environments for cell culture so that the natural environment, 3D architecture, cell morphologies and polarity seen *in vivo* can be maintained. Technologies that are low cost and practical, and which ensure high reproducibility and better control over spheroid diameters [21] are of great interest.

Poly (N-isopropylacrylamide) (PNIPAm) is a thermosensitive and biocompatible polymer frequently used in drug delivery and as biomimetic substrates for cell sheet engineering applications [22-25]. PNIPAm undergoes reversible changes in its physicochemical properties at 32-35°C, which is known as its critical phase transition temperature (Tp) or lower critical solution temperature (LCST) [26]. PNIPAm hydrogels are hydrophobic above LCST, which facilitates cell attachment, and their surfaces become hydrophilic below LCST, which leads to the detachment of cells. This thermoresponsive detachment of the cells occur in a manner that avoids cell membrane damage and maintains the cell-to-cell integrity without loss of basal ECM proteins [26]. Furthermore, PNIPAm-based crosslinked hydrogel surfaces have been shown to mimic the physicochemical and mechanical characteristics of the ECM, thus providing an environment that imitates native milieus for the attachment and growth of cells [27]. These properties make PNIPAm an attractive material for the culture and stress-free isolation of 3D cell spheroids in a biomimetic environment unlike other 3D spheroid culture techniques in use today. The reversible changes in the properties of PNIPAm can be attributed to its coil-to-globule transition that occurs near LCST. Below LCST, the hydrophilic amide groups of NIPAm form hydrogen bonds with the surrounding water molecules, resulting in a well-solvated random-coil conformation. However above LCST, the hydrophobic regions (isopropyl groups) of NIPAm chains are exposed, and the polymer collapses leading to squeezing out of hydrogen-bonded water molecules and the adoption of a globule-like conformation, and causing the de-swelling of NIPAm above LCST [28-30]. In cell sheet and tissue engineering, PNIPAm provides an excellent substrate for the attachment, proliferation, and aggregation of cells at 37°C [31], and allows cell or cell sheet detachment via a simple temperature switch, without the use of trypsin. Previously, cell spheroids have been cultured inside PNIPAm-based hydrogels, and these were released at temperatures <LCST when the hydrogels liquified [32,33]. However, this method does not offer control over the diameters of the spheroids formed, which can lead to batch-to-batch variability. We demonstrate a unique method of developing PNIPAm-based hydrogel microwell arrays (PHMA), which can be used for high-throughput generation of spheroids of relatively uniform diameters. To the best of our knowledge, there are no studies where PNIPAm hydrogel microwell arrays have been used for spheroid generation. This study confirms the versatility of the PHMAs in terms of generating spheroids using different cell types including epithelial cells, fibroblasts and osteoblast cells. Spheroid development

within the PHMAs was optimized for seeding density, incubation time and cell viability, and the spheroids were then used for preliminary anti-cancer drug screening studies. The proposed PHMAs provided a bioinspired environment for cell spheroids to attach and grow, unlike 3D cell culture methods that employ non-adhesive surfaces for spheroid formation.

2. MATERIALS AND METHODS

2.1 Design and fabrication of the negative micromold:

3D computer aided design (CAD) software (SolidWorks software, Dassault Systemes, USA) was used to first design a negative micromold (Figure 1B), with 11 × 11 cylinders of desired dimensions (diameters and height: 800 μm) (Figure 1A), so that PHMAs with microwells of corresponding dimensions could be cast using them. The negative micromold was then 3D printed (Proto Labs, Inc. MN, USA) using Accura Xtreme White material, as shown in Figure 1C.

2.2 Formulation of PHMA:

All chemicals were purchased from Sigma-Aldrich, USA and used without further purification. First, 10% w/v N-isopropylacrylamide (NIPAM), 0.4% w/v N,N′-methylenebisacrylamide (BIS), 1% w/v Ammonium persulphate (APS), 0.11% w/v acrylic acid (AA) and N,N,N′,N′,-Tetramethylethylenediamine (TEMED) were dissolved sequentially in deionized (DI) water. The final polymer mixture was immediately poured onto the negative micromold and left undisturbed at room temperature (RT) overnight for gel formation. Following gelation, the PHMA was alternately subjected to heat (37°C) and cold (4°C) treatment in water for 12 hours at each temperature, to facilitate easy detachment and to wash out excess chemicals.

The detached PHMAs were transferred to a new container and stored in excess water at 4°C until further use. Schematic representation of fabrication of PHMA and its application in the generation of spheroids is shown in Figure 2.

2.3 Characterization of PHMA

To visualize the microwells within the PHMA, EVOS® FL imaging (Life Technologies corporation, Bothell WA, USA) was done at 25°C and 37°C, and scanning electron microscopy (SEM, Zeiss Sigma, USA) was also performed. For SEM, the PHMAs were dehydrated using a series of alcohols (50, 60, 70, 80, 90 and 100 % v/v ethanol diluted in PBS) for 5 mins at each step followed by air drying for 24h. Following this, the gel sample was placed on the stub using double sided carbon tape and sputter coated with gold before imaging.

2.3.1 Swelling behavior: Swelling properties of formulated PHMA was determined by immersing the freeze-dried PHMA in deionized water at RT. Swollen hydrogel samples were weighed by an electronic balance at predetermined time points after wiping the excess water on the surface using filter paper [34]. The swelling ratio (SR) was calculated by the following equation 1, where Ws is the weight of the swollen sample at time t (days 1-7) and Wd is the weight of the freeze-dried sample at time t=0.

$$SR = \frac{Ws - Wd}{Wd}$$

2.3.2 Shrinking behavior (Temperature dependence studies): Temperature-dependent shrinking behavior of the PHMA was evaluated by sequentially increasing the temperature from 20°C to 45°C at 5°C increments, after achieving equilibrium at each targeted temperature. The desired temperature was controlled by a thermostatic water bath. At each temperature, the samples were blotted dry with filter paper before weighing [34]. The shrinking ratio was recorded using equation 1 as shown above.

2.3.3 De-swelling Kinetics: De-swelling kinetics of the PHMA were assessed by immersing the freeze-dried samples in de-ionized (DI) water at 25°C for 5 days. After 5 days, the equilibrium swollen hydrogels were then transferred to DI water at 45°C. At predetermined time points, the samples were removed and blotted with filter paper before weighing [34]. Water retention (WR) was calculated according to equation 2, where Wt is the weight of the shrunken PHMA at specific time t at 45°C, Wd is the weight of the freeze-dried hydrogel, and We is the weight of the equilibrium swollen hydrogel at 25°C.

$$Percent\ WR = \frac{Wt - Wd}{We - Wd} * 100$$

2.3.4 Re-swelling degree: To study the reversible swelling/ de-swelling behavior of PHMAs, re-swelling test was performed by moving gels equilibrated at 45°C to deionized water at 25°C. At predetermined time points, the swollen PHMA were removed and dried by using filter paper before weighing[34]. Re-swelling degree (RD) was calculated using equation 3, where Wr is the weight of re-swelling PHMA at specific time and We is the weight of the equilibrium swollen PHMA at 25°C.

$$Percent\ RD = \frac{Wr}{We} * 100$$

2.3.5 LCST behavior: A thermogram was obtained using differential scanning colorimetry (DSC, TA instruments Q100) by scanning the sample in the temperature range of −40°C to 60°C with a rate of 2°C/min. Temperature-dependent changes in visual appearance of the PHMA was also recorded.

2.3.6 Contact angle measurements: Hydrophobicity of the developed PHMA was determined by contact angle measurements using ImageJ. Specifically, hydrogels at different temperatures were prepared in a 48-well plate and placed upright. A 300 μL drop of DI water was then added onto the surface of each hydrogel. The drops were captured with a camera using the same objective lens at the same distance of 3 feet. Finally, the images were analyzed on ImageJ using the Contact Angle plug-in, with the setting of manual border selection and at least 30 points were randomly selected on each image.

2.4 *In vitro* evaluation of PHMA for spheroid generation

For all *in vitro* experiments, the PHMAs were initially kept in DI water at 37°C for around 4-5 h to shrink, following which they were sterilized using 70% ethanol for 2 min and immediately transferred to well plate. The PHMAs were then incubated in complete Dulbecco's modified eagle's medium (DMEM supplemented with 10% fetal bovine serum (FBS) and 1% Penicillin-streptomycin) (Sigma-Aldrich, USA) for one day at 37°C to equilibrate them. Immediately prior to cell culture experiments, the DMEM was removed. Fresh DMEM was added during cell seeding.

2.4.1 Cell seeding optimization for the formation of spheroids: To optimize cell seeding densities, we used HeLa cervical adenocarcinoma cells as the model cell line. HeLa cells at different seeding densities (8×10^4, 24×10^4 and 72×10^4 cells/PHMA) were added to the equilibrated PHMA placed in a 6-well plate and cultured in complete DMEM. The media was replaced every 3 days. At predetermined time points (1, 3, 5 and 7 days), WST-1 assays (Sigma-Aldrich, USA) were carried out following manufacturers' instructions. Further Live/Dead™ assay (Invitrogen, Carlsbad, CA) was done as per manufacturers' directions to evaluate cell viability.

2.4.2 Formation of spheroids: To demonstrate the feasibility of using the PHMA for generating spheroids with different cell lines, A549 lung cancer epithelial cells (ATCC® CCL-185™ Manassas, VA, USA), MG-63 bone sarcoma cells (ATCC® CRL-1427™ Manassas, VA, USA), and human lung fibroblasts (HLFs-ATCC® PCS-201-013™ Manassas, VA, USA) were also cultured separately within the PHMA. A549 and MG-63 cells were cultured in complete DMEM media while HLFs were cultured in fibroblast basal media supplemented with low serum and nutrients recommended by ATCC (fibroblast growth kit-low serum ATCC® PCS-201-041™, Manassas, VA, USA) and 1% penicillin-streptomycin. In this experiment, the cells were seeded at the optimized density of 24×10^4 cells/PHMA. At predetermined time points (1, 3, 5 and 7 days), brightfield EVOS imaging and Live/Dead analysis (Calcein AM and Ethidium homodimer-1 (ED-1) (Thermo Fisher Scientific, Waltham, MA, USA) of the spheroids was performed.

2.4.3 Evaluation of hypoxic core development within the spheroids: The different morphologies of spheroids for different cell lines are expected to be different due to the inherent properties of the cells, as reported previously [35]. For example, distorted morphologies are commonly observed for A549 spheroids [36] while spherical and intact morphologies are observed for MG-63 spheroids [37]. Due to the compact and spherical morphology of MG-63 spheroids, this cell line was used for further investigation. MG-63 cells at a density of 24×10^4 cells/PHMA were seeded in the PHMA and spheroids were cultured for 5 days. They were then washed and fixed with 3.7% paraformaldehyde and 2% sucrose in PBS for 2 hours at RT. Spheroids were washed with ice cold PBS followed by permeabilization using 0.3% Triton-X-100 for 15 minutes at RT. They were washed thrice with ice cold PBS, and blocking was carried out using 0.5% Goat serum (Southern Biotech, catalog number-0060-01) and 0.1% NP-40 in PBS. Spheroids were incubated for 6 hours with rabbit anti-human HIF1α antibody (Bethyl Antibodies, catalog number-A300-286A) in blocking solution. The HIF1α stained spheroids were then incubated with a goat anti-Rabbit

conjugated highly cross-adsorbed antibody (Thermo Fisher Scientific, Alexa Fluor 488, catalog number-A-11008) diluted in blocking solution at RT for 2 hours. All spheroids were then washed and incubated with 3μg/ml DAPI in PBS (stock 1 mg/ml) for 15 minutes to stain the nucleus. Brightfield and fluorescent images were captured using an inverted confocal microscope (Zeiss Confocal, SPOT Imaging). All image analyses were conducted using the Zeiss imaging software.

2.4.4. Anti-cancer drug screening using spheroids generated with PHMAs: In this proof-of-concept drug response study, doxorubicin hydrochloride (Dox, Sigma-Aldrich, USA), which is frequently used in osteosarcoma chemotherapy, was tested against the MG-63 spheroids [38]. The optimized seeding density of 24×10^4 cells/PHMA was used to generate MG-63 spheroids in the PHMA. Cells were incubated for 5 days to form the spheroids. After 5 days of incubation, the MG-63 spheroids were treated with 1, 5 and 10 μM concentration of Dox solubilized in media, based on IC_{50} values noted previously [39-41]. The effect of Dox was evaluated at 24, 48 and 72h following treatment. At these time points, the PHMA containing MG-63 spheroids were imaged using EVOS and confocal microscopy. At 72h, 3D CellTiter-Glo® luminescent cell viability assay (Promega Corporation, USA) was employed to evaluate the percent cell viability of Dox-treated spheroids and compared with the control (untreated) group.

3. RESULTS

3.1 Development of PHMA:

In the present investigation, the PHMAs were successfully synthesized using a customized negative micromold. The dimensions of the columns in the micromold (diameter and height of 800 μm) are larger than what is generally implemented in conventional microwell array templates [42,43] to allow for the PNIPAm to shrink at LCST and still maintain well space for spheroid growth.

3.2 Characterization of PHMA:

Formulated PHMA were evaluated for their thermoresponsive behavior, and swelling, shrinking, reswelling, and deswelling kinetics. SEM images of the PHMA show spherical and uniform well diameters with smooth surfaces (Figures 3A and B). As shown in Figures 3C and E, we observed a change in the color of PHMA from colorless to white when the temperature was increased from 25°C to 37°C.

EVOS imaging confirmed that the diameters of the wells in PHMA decreased from 800 μm to 550 μm when the temperature increased from 25°C to 37°C (Figure 3D and F). The DSC thermogram of PHMA also clearly showed an endothermic peak at 34.62°C, indicating that this is the LCST of the construct (Figure 3G).

From Figures 4A and B, it is obvious that the contact angle of the water drops on PHMA increased with the increase of temperature, indicating that the hydrogel became more hydrophobic. At 37°C, the contact angle increased to almost 90°, indicating that the PHMA became hydrophobic at physiological temperature, while it remains relatively hydrophilic at room temperature and below.

The swelling behavior of PHMA in deionized water at 25°C is shown in Figure 5A. The samples underwent swelling on day 1 and then plateaued, leading to no further change in weight to day 6. As shown in Figure 5B, the PHMA demonstrated temperature-dependent shrinking, and achieved maximum shrinking above 35°C. The de-swelling kinetics of the PNIPAm is shown in Figure 5C. When transferred from 25 to 45°C, the PHMA demonstrated rapid shrinking and decreased water retention, and its weight was stabilized within about 50 mins. Re-swelling property of thermosensitive material is critical to ensure that the PHMA can undergo phase transition to allow for spheroid detachment at RT. The re-swelling degree was measured by decreasing the surrounding temperature of the gels from 45°C to 25°C. The graph shown in Figure 5D reveals that the PHMA re-swelling percentage of the gel was 49 ± 4.8% in 180 minutes.

3.3. *In vitro* studies using PHMA

3.3.1. Optimization of cell seeding density for the formation of spheroids: Cell seeding optimization was performed by determining spheroid viability over 14 days using WST-1 formazan-based assays and imaging the spheroids over one week.

EVOS images of HeLa spheroids in PHMA seeded at the lowest seeding density of 8×10^4 cells/PHMA shows intact spheroid formation by day 7. With a seeding density of 24×10^4 cells/PHMA, spheroids are formed by day 5 with a distinctly dark core, indicating possible development of hypoxia [44,45]. For this seeding density, the cells began to aggregate by day 3, and intact multicellular spheroid formation with clear morphologies was observed by day 5. The seeding density of 72×10^4 cells/PHMA resulted in cells taking up the entire well space within the PHMA on day 1 and forming highly dense spheroids by day 3 (Figure 6A). WST-1 assays confirmed that these supersaturated spheroids had decreased cell viability on day 4. With the lowest seeding density of 8×10^4 cells/PHMA, cell proliferation and viability increased up to day 8, and then saturated. With the 24×10^4 cells/PHMA density, an increase in viability was observed until day 3, which then remained constant as the cells rearranged themselves to form compact spheroids as seen in the EVOS images (Figure 6B). Therefore 24×10^4 cells/PHMA was considered as optimum cell seeding density for future experiments.

3.3.2. Spheroid generation using different cell lines: To demonstrate the broad applicability of the novel PHMA for the development of spheroids using different cell types, we cultured human epithelial cancer cells (A549 and HeLa), osteoblast like cells (MG-63) and fibroblast cells (HLF) within the PHMAs. The optimized seeding density of 24×10^4 cells/ PHMA was used. EVOS images depicted in Figure 7 confirm successful formation of spheroids with all cell lines.

HLF spheroids demonstrated spherical morphology, and the diameter decreased slightly until day 5 as the cells were rearranged to form spheroids with compact morphology. MG-63 cells formed spherical spheroids on day 1 and the spheroid diameter and compactness increase with time until day 7. A549 cells took longer to form spheroids, and these spheroids had comparatively more distorted morphology than the other cell lines.

The viability of the generated spheroids at 24 × 10^4 cells/ PHMA density on day 7 were analyzed using Live/Dead™ assays. Representative EVOS fluorescent microscopic images are shown in Figure 8. Green fluorescence from the periphery of the spheroids indicated that the cells in the periphery stained green by Calcein AM were metabolically active and viable. Red staining would indicate presence of ED-1, which tends to bind to nucleic acids of ruptured dead cells [46]. No red fluorescence was observed from within the spheroids.

3.3.3. Evaluation of hypoxic core development within the spheroids: To confirm the development of hypoxic cores similar to those seen in large tumors *in vivo*, MG-63 spheroids cultured for 5 days were immunostained for HIF-1α expression, and DAPI was used to stain the nucleus. Cross-sections of stained spheroids obtained using confocal microscopy clearly show development of foci of HIF-1α (green) within the spheroid (Figure 9). The HIF-1α protein was found to localize internally in the core of the spheroid, suggesting that the outer layer of cells in spheroid were normoxic while the central core is hypoxic.

3.3.4. Anti-cancer drug screening using spheroids generated with PHMAs: Spheroid cultures are being increasingly used in anti-cancer drug screening studies, as reported previously [47,48], as they recapitulate *in vivo* environments more accurately than 2D cultures. Since MG-63 spheroids were comparatively intact and spherical with closely packed cells, it would be easier to visualize changes in spheroid morphology in response to drug treatment. Therefore, a proof-of-concept drug response study was carried out using MG-63 spheroids cultured up to day 5. The spheroids were treated with 1, 5 and 10 μM concentration of Dox [49] and the effects of the treatment on cell viability were determined. The Cell Titer Glo assay clearly indicated cell death upon treatment with all the three concentrations of Dox when compared with the control group (Figure 10A). Exposure of Dox to MG-63 spheroids demonstrated concentration-dependent cell death i.e. 39.2 ± 7.4% viability for 1 μM and 24.2 ± 2.9% for 10 μM treatment. The uptake of Dox in MG-63 spheroids was evaluated after 24 (Figure 10B), 48 (Figure 10C) and 72h (Figure 10D) by confocal microscopy.

We observed a time- and concentration- dependent accumulation of Dox within the spheroids. After 24h of treatment, the fluorescence from the Dox was clearly visible within the cell spheroids treated with 10 μM Dox, while the other treatment groups had comparatively lower fluorescence intensity. However, after 72h, Dox fluorescence was observed throughout the spheroid for all Dox concentrations, with the highest intensity at 10 μM concentration.

4. DISCUSSION

We report the development of an innovative thermoresponsive hydrogel microwell array using PNIPAm - a well-known thermosensitive polymer with LCST in the range of 32-35°C [26]. The fundamental thermoresponsive property of PNIPAm polymer has already been exploited in cell sheet engineering where cells growing on the PNIPAm surface form detachable cell sheets when the temperature is switched from 37°C to RT [50,51]. In the present investigation, NIPAm and AA were copolymerized to form the microwell arrays. AA

is a source of negatively charged carboxylic groups, which prevents the polymer chains from aggregating at RT and facilitates swelling of the PHMA [32]. The developed PHMA demonstrated thermoresponsive phase transition above 35°C. SEM images of the PHMA showed spherical wells of uniform diameters with smooth internal surfaces for cell attachment. As has been shown by previous studies, spheroids with diameters in the range of 400-500 μm are optimal for representing tumors observed *in vivo*, with an external proliferating zone and an internal quiescent zone [52-54]. Therefore, the diameters of the microwells within the PHMA are appropriate for forming spheroids within this range. The DSC thermogram confirmed the LCST of PHMA to be 35°C. Phase transition was also established by contact angle studies which clearly shows that the contact angle increased to about 83° at 37°C, indicating that the PHMA became hydrophobic at physiological temperature, while it remains relatively hydrophilic at RT and below. Although the term "hydrophobic" is considered for contact angle θ>90°, this is usually applicable to solid surfaces; since the PHMA is hydrated, the hydrophobicity of our gel is influenced by the hydrophobic nature of PNIPAm above LCST, as well as the presence of water within the gel. The trend of increasing hydrophobicity of PNIPAm as temperature increases above LCST is in line with reported literature, where static contact angle θ increased from 36° to 46° for PNIPAm brush [55] and from 64° to 94° for silicon-coated PNIPAm brush [56]. Conzatti et al. has also reported the same trend of hydrophilic/hydrophobic transition near LCST for PNIPAm-based hydrogels [57]. The maximum swelling of PHMA within 24 h could be attributed to the polymer density and the hydrophilic property of AA used in the formulation, which increased the affinity of PHMA towards water [32,58]. Swelling ratios of PHMA could be controlled by varying the ratio of AA to NIPAM monomer.

Deswelling studies showed stabilization of the PHMA within about 50 mins. This property is very important as the de-swelling and subsequent increase in hydrophobicity of the PNIPAm surface is necessary for cell attachment and proliferation to form spheroids. Deswelling behavior of PHMA is mainly dependent on the presence of hydrophilic content and the density of the monomer NIPAm. Polymerization of the hydrophilic AA with PNIPAm can lead to the generation of water releasing channels [32,58], and the entrapped water molecules in the PHMA are released when they are exposed to temperatures >LCST. Re-swelling property of the thermosensitive material is critical to ensure that the PHMA can undergo phase transition to allow for spheroid detachment at RT. After swelling, the surface of the PHMA is expected to become hydrophilic making it suitable for the detachment and isolation of cells as described previously [32,50,51,58]. The mechanical strength of the PHMA was also analyzed, and the platform was found to have sufficient stiffness to enable cell culture within it (see Supplementary information).

Following thorough characterization, the PHMA was then used for spheroid generation. WST-1 assays and EVOS imaging using HeLa spheroids confirmed 24×10^4 cells/PHMA as a suitable cell seeding density for future experiments. This seeding density was optimized based on the morphology of spheroids and quantitative cell viability assays showing the percentage of viable cells overtime. Seeding density can be further optimized for each cell line used and based on the dimensions of the microwells. Studies performed by Lei et al., clearly demonstrated the development of HeLa spheroids of 226, 267 and 388 μm diameters when seeded at 5×10^6 cells/reservoir in wells of diameter 400, 600 and 800 μm after 4 days

[59]. Similarly, Barros et al., reported the development of HeLa spheroids of 662.6 ± 70 μm diameter in 10 days when seeded at 1×10^6 cells/ agarose micromold [60]. We see the development of compact HeLa spheroids within the PHMA within similar timeframes. The spheroids grown within the PHMA could be easily isolated following temperature-dependent phase transition at RT, as shown for day 7 in Figure 5A. Each customized PHMA can be placed within the well of a 6 well plate for the high-throughput generation of relatively uniform spheroids in an environment that more closely mimics cellular attachment and grown on ECM *in vivo*. To validate the broader utility of the developed PHMA model, 3D spheroids were also generated using A549, MG-63 and HLF cell lines. HepG2 hepatocellular carcinoma cell line was also seeded into the PHMA at a seeding density of 25×10^4cells/ PHMA and were found to form spheroids with compact, relatively spherical morphologies after day 5 (Figure S1).

The ability of spheroids to recapitulate several key chemical and physical properties seen *in vivo* such as oxygen tension (hypoxia in spheroids), compactness (cell to cell interaction), and gene and protein expression, makes them a suitable alternative to animal model testing, which is the current gold standard in preclinical drug development. Cell spheroids and organoids are being increasingly used for predictive evaluation of new anti-cancer therapeutics including chemotherapy, antibody-based immunotherapy, gene therapy and combinatorial therapies [61]. It is well known that the ECM and compact cell arrangement can act as key barriers hindering the penetration of therapeutics into the tumor. Inability to recapitulate these barriers in 2D monolayer culture systems is potentially the reason why nanoparticles/ drugs demonstrating high efficacy on 2D cell cultures fail to show similar effects with 3D cell spheroids [62,63]. Studying drug penetration kinetics using spheroids can also provide valuable information to researchers which will enable them to modify their formulations to increase penetration into the diseased tissues. For example, Conte et al developed novel redox-responsive PLGA (poly(lactic-co-glycolic acid))-PEG (polyethylene glycol) nanoparticles (RR-NPs) and compared them to corresponding non-redox-responsive nanoparticles (nRR-NPs) in terms of penetration ability into A549 spheroids. Significant penetration of RR-NPs was achieved through all regions of the spheroids (the outer proliferating zone, the middle viable layer of quiescent cells and the central necrotic core) when compared to nRR-NPs [64]. Disease-specific cell marker expression is usually recapitulated more accurately by 3D cell spheroids than by 2D monolayer cultures. Several studies have reported expression of cell markers varies significantly when exposed to the inducing agent on 2D and 3D cell system. For example, lipopolysaccharide-induced secretion of pro-inflammatory cytokine response was found to be significantly different between 2D and 3D cell systems. A549 cell spheroids demonstrated persistently increased levels of interleukin-6 and interleukin-8 compared with its corresponding monolayer cultures [65]. Toxicology is yet another area in which the use of spheroids has shown clear advantages over 2D assays. Bell *et al.* conducted a multi-center comparison of 2D sandwich cultures and 3D spheroids of primary human hepatocytes (PHHs) over two weeks in order to evaluate their suitability for long-term *in vitro* toxicology assays, comparing both to a baseline of freshly-thawed and -plated PHHs. Their work found that spheroids tended to retain or upregulate the stable synthesis of metabolic proteins, over a 14-day period while 2D cultures rapidly lost this ability. 2D cultures were also observed to lose the ability to

express various proteins involved in drug absorption, distribution, metabolism, and excretion (ADME), and experienced a relatively rapid rise in the expression of degradative proteins (*e.g.*-lysosomal proteins). Spheroids were found to be more sensitive to subtle toxicological differences, shown by their ability to discriminate between the toxicological profiles of troglitazone and its less toxic analog pioglitazone [66]. Thoms *et al.* carried out similar comparative work between standard 2D culture and spheroids to address the underestimation of tacrolimus toxicity *in vitro* compared to that observed *in vivo* in patients. They found that 3D spheroids were able to better predict this toxicity, and like so many others in recent years, advocated the adoption of these physiologically more relevant models for such toxicological work [67].

To visualize the morphologies of our developed spheroids, EVOS imaging was also done. The HLFs formed spheroids with spherical and compact morphologies. Fibroblast spheroids are useful building blocks for forming large multicellular constructs of different tissues. Cancer-associated fibroblasts are known to play a key role in the growth and invasion of many tumors [68] and are therefore increasingly being co-cultured with cancer cells *in vitro*. Our studies confirm that fibroblasts can be cultured in a 3D format within the PHMA. Primary human fibroblasts tend to form spherical intact microtissues as demonstrated previously [69,70]. Spheroids developed using MG-63 cells demonstrated increasing diameter and compactness with time until day 7, as also observed by other groups under normoxic conditions[6,71]. The comparatively more irregular morphology of A549 cell spheroids developed within the PHMA is also consistent with previous reports on developing spheroids using A549 cells [72,73]. Sambale et al.[74] reported that A549 cells demonstrated lower cell-to-cell interactions compared to fibroblasts, leading to the generation of loosely packed spheroids. The differences in the overall morphology of the cell spheroids could be attributed to the differences in their cell-cell adhesion properties. It is well-documented that cell-to-cell adhesion is a key step in tissue development and regulates morphology, polarity, and tissue integrity. Cadherins, especially E-cadherins, are known to play a key role in promoting cell adhesion. The presence of E-cadherins prevents dissociation and migration of most non-cancer cells, particularly epithelial cells, from the original tissue [75-77]. In this study, HLF spheroids were spherical with intact periphery, and EVOS images indicated that no visual changes in diameter were noted after day 5. On the other hand, cancer cells within spheroids progressively lose the ability to maintain a compact structure and hence form larger and distorted tissue constructs indicating loss of E-cadherin. This loss of E-cadherin is more common in cancers of epithelial origin, such as A549 and HeLa [75]. There have been several studies which suggest that the downregulation of E-cadherin reduces cell-cell adhesion, and increases epithelial to mesenchymal transition which is commonly seen in cancer [76,77].

Following characterization of the morphologies of the spheroids, the development of hypoxic core within them was also studied using EVOS and confocal imaging. Hypoxia is a common phenomenon seen in malignant tumors and signifies lower level of oxygen tension in a specific tissue. In normal tissues, the clinical median percent O_2 level is in the range of 3.9-9.5 (normoxic condition) whereas tumor tissues show a median O_2 levels in the range of 0.3 – 1.8 (hypoxic conditions) [78,79]. This hypoxic condition in tumor tissue leads to abnormal vascularization and metastasis and subsequently causes altered cancer cell

metabolism. Hypoxia-inducible factors (HIF) are key transcription factors in the mammalian response to oxygen deficiency [80]. During hypoxia, HIF-1α levels in the nucleus is stabilized. Together with other transcription factors, HIF-1α play key roles in many crucial aspects of cancer biology including angiogenesis [81], epithelial-mesenchymal transition [82], invasion [83] and metastasis [84]. Further, hypoxia in tumor microenvironments induces cellular changes that make these cells highly resistant to chemotherapy, immune and radiation therapy [85]. In the present investigation, MG-63 spheroids clearly show the localization of HIF-1α protein in the internal core suggesting that the central core is hypoxic. The results are consistent with the existing literature on tumor microenvironments and spheroid development, which shows that the complex architecture of tumor tissue leads to limited access of oxygen to the tumor cells in the center [86]. During the development of spheroids, the outer layer, also known as the proliferating zone, has access to nutrients and oxygen while the cells in the center have access to limited oxygen [86,87]. Further, the increased oxygen diffusion distance in spheroids with increasing diameters ultimately reduces the availability of oxygen and leads to poor diffusion of media towards the center of the spheroid [88]. Our results are consistent with previous research, where MG-63 spheroids where hypoxia induction and HIF-1α protein expression was observed in spheroids of small diameters [89,90].

Following successful characterization of MG-63 spheroids, a proof-of-concept Dox response study was carried out. Confocal images and Cell Titer Glo assays clearly demonstrated the time- and concentration-dependent uptake of the Dox by the spheroids. HIF-1α expression has been previously shown to mediate multi drug resistance phenotype in MG-63 cells upon Dox treatment [91]. In this work, we have successfully demonstrated that 3D hypoxic environments can be generated in the core of MG-63 spheroids in the PHMAs. Therefore, the responses of these spheroids to chemotherapies like Dox are expected to be more representative of *in vivo* responses than 2D monolayer cultures which cannot be used to recapitulate hypoxic cores seen in tumors *in vivo*. To the best of our knowledge, this is the first report on the development of thermoresponsive PNIPAm hydrogel microwell arrays for spheroid generation and isolation. Future studies will focus on investigating the suitability of PHMA for generating multicellular spheroid co-cultures and for the development of spheroids using human patient-derived cells. These models will more closely mimic *in vivo* disease conditions for predictive drug screening.

5. CONCLUSIONS

We report for the first time the development of a unique PNIPAm-based hydrogel microwell array for the easy generation and isolation of spheroids with uniform morphology. The optimized seeding density for the generation of HeLa spheroids was found to be 24×10^4 cells/PHMA. The developed PHMA was also used for the generation of A549, MG-63 and HLF spheroids. As a proof-of-concept, the responses of the developed MG-63 spheroids to Dox treatment were studied. Drug penetration and anticancer efficiency was found to be dependent on the Dox concentration and time. To the authors' knowledge, this is the first report on the development of PNIPAm hydrogel-based microarray models for the generation of cell spheroids in a biomimetic environment for use in *in vitro* drug testing and to study mechanisms associated with disease progression.

Supplementary Material

Refer to Web version on PubMed Central for supplementary material.

Acknowledgment

We would also like to acknowledge Imaging facility at the RI Consortium for Nanoscience and Nanotechnology, a URI College of Engineering core facility partially funded by the National Science Foundation EPSCoR, Cooperative Agreement #OIA-1655221. The authors would also like to thank Dr. Carlos Javier for helping us in making the software copy of our design.

Funding Sources

This work was supported by the Rhode Island Institutional Development Award (IDeA) Network of Biomedical Research Excellence from the National Institute of General Medical Sciences of the National Institutes of Health under grant number P20GM103430.

REFERENCESReference List

[1]. DiMasi JA, Grabowski HG, Hansen RW, Innovation in the pharmaceutical industry: new estimates of R&D costs, J. Health Econ 47 (2016) 20–33. [PubMed: 26928437]

[2]. Begley CG, Ellis LM, Raise standards for preclinical cancer research, Nature. 483 (2012) 531–533. [PubMed: 22460880]

[3]. Kuriakose AE, Hu W, Nguyen KT, Menon JU, Scaffold-based lung tumor culture on porous PLGA microparticle substrates, PloS one. 14 (2019) e0217640. [PubMed: 31150477]

[4]. Stock K, Estrada MF, Vidic S, Gjerde K, Rudisch A, Santo VE, Barbier M, Blom S, Arundkar SC, Selvam I, Capturing tumor complexity in vitro: Comparative analysis of 2D and 3D tumor models for drug discovery, Scientific reports. 6 (2016) 1–15. [PubMed: 28442746]

[5]. Halfter K, Mayer B, Bringing 3D tumor models to the clinicâ€“predictive value for personalized medicine, Biotechnology journal. 12 (2017) 1600295.

[6]. Anada T, Masuda T, Honda Y, Fukuda J, Arai F, Fukuda T, Suzuki O, Three-dimensional cell culture device utilizing thin membrane deformation by decompression, Sensors Actuators B: Chem. 147 (2010) 376–379.

[7]. Wegert J, Zauter L, Appenzeller S, Otto C, Bausenwein S, Vokuhl C, Emestus K, Furtwängler R, Graf N, Gessler M, High-risk blastemal Wilms tumor can be modeled by 3D spheroid cultures in vitro, Oncogene. (2019) 1–13.

[8]. Rashidi MRW, Mehta P, Bregenzer M, Raghavan S, Fleck EM, Horst EN, Harissa Z, Ravikumar V, Brady S, Bild A, Engineered 3d model of cancer stem cell enrichment and chemoresistance, Neoplasia. 21 (2019) 822–836. [PubMed: 31299607]

[9]. Raghavan S, Ward MR, Rowley KR, Wold RM, Takayama S, Buckanovich RJ, Mehta G, Formation of stable small cell number three-dimensional ovarian cancer spheroids using hanging drop arrays for preclinical drug sensitivity assays, Gynecol. Oncol 138 (2015) 181–189. [PubMed: 25913133]

[10]. Zhao L, Xiu J, Liu Y, Zhang T, Pan W, Zheng X, Zhang X, A 3D Printed Hanging Drop Dripper for Tumor Spheroids Analysis Without Recovery, Scientific reports. 9 (2019) 1–14. [PubMed: 30626917]

[11]. Cho C, Chiang T, Hsieh L, Yang W, Hsu H, Yeh C, Huang C, Huang J, Development of a Novel Hanging Drop Platform for Engineering Controllable 3D Microenvironments, Frontiers in Cell and Developmental Biology. 8 (2020) 327. [PubMed: 32457907]

[12]. Lee T, Bhang SH, La W, Yang HS, Seong JY, Lee H, Im G, Lee S, Kim B, Spinner-flask culture induces redifferentiation of de-differentiated chondrocytes, Biotechnol. Lett 33 (2011) 829–836. [PubMed: 21125413]

[13]. He H, He Q, Xu F, Zhou Y, Ye Z, Tan W, Dynamic formation of cellular aggregates of chondrocytes and mesenchymal stem cells in spinner flask, Cell Prolif. 52 (2019) e12587. [PubMed: 31206838]

[14]. Costa EC, de Meloâ€• Diogo D, Moreira AF, Carvalho MP, Correia IJ, Spheroids formation on nonâ€• adhesive surfaces by liquid overlay technique: Considerations and practical approaches, Biotechnology journal. 13 (2018) 1700417.

[15]. Leary E, Curran S, Susienka M, Manning KL, Blakely AM, Morgan JR, Micromoulded non-adhesive hydrogels to form multicellular microtissues–the 3D Petri Dish®, Technology Platforms for 3D Cell Culture. (2017) 97–122.

[16]. Lee JM, Choi JW, Ahrberg CD, Choi HW, Ha JH, Mun SG, Mo SJ, Chung BG, Generation of tumor spheroids using a droplet-based microfluidic device for photothermal therapy, Microsystems & Nanoengineering. 6 (2020) 1–10.

[17]. Tomasi RF, Sart S, Champetier T, Baroud CN, Individual Control and Quantification of 3D Spheroids in a High-Density Microfluidic Droplet Array, Cell reports. 31 (2020) 107670. [PubMed: 32460010]

[18]. Järvinen P, Bonabi A, Jokinen V, Sikanen T, Simultaneous Culturing of Cell Monolayers and Spheroids on a Single Microfluidic Device for Bridging the Gap between 2D and 3D Cell Assays in Drug Research, Advanced Functional Materials. 30 (2020) 2000479.

[19]. Stetler-Stevenson WG, Aznavoorian S, Liotta LA, Tumor cell interactions with the extracellular matrix during invasion and metastasis, Annu. Rev. Cell Biol 9 (1993) 541–573. [PubMed: 8280471]

[20]. Dutta RC, Dutta AK, Comprehension of ECM-Cell dynamics: A prerequisite for tissue regeneration, Biotechnol. Adv 28 (2010) 764–769. [PubMed: 20600786]

[21]. Tang Y, Liu J, Chen Y, Agarose multi-wells for tumour spheroid formation and anti-cancer drug test, Microelectronic Engineering. 158 (2016) 41–45.

[22]. Nash ME, Healy D, Carroll WM, Elvira C, Rochev YA, Cell and cell sheet recovery from pNIPAm coatings; motivation and history to present day approaches, Journal of Materials Chemistry. 22 (2012) 19376–19389.

[23]. Menon JU, Kuriakose A, Iyer R, Hernandez E, Gandee L, Zhang S, Takahashi M, Zhang Z, Saha D, Nguyen KT, Dual-drug containing core-shell nanoparticles for lung cancer therapy, Scientific reports. 7 (2017) 1–13. [PubMed: 28127051]

[24]. Sundaresan V, Menon JU, Rahimi M, Nguyen KT, Wadajkar AS, Dual-responsive polymer-coated iron oxide nanoparticles for drug delivery and imaging applications, Int. J. Pharm 466 (2014) 1–7. [PubMed: 24607216]

[25]. Yadavalli T, Ramasamy S, Chandrasekaran G, Michael I, Therese HA, Chennakesavulu R, Dual responsive PNIPAM–chitosan targeted magnetic nanopolymers for targeted drug delivery, J Magn Magn Mater. 380 (2015) 315–320.

[26]. Okano MNT, Winnik FM, Poly (N-isopropylacrylamide)-based smart surfaces for cell sheet tissue engineering, Material Matters. 5 (2010) 56.

[27]. Capella V, Rivero RE, Liaudat AC, Ibarra LE, Roma DA, Alustiza F, Mañas F, Barbero CA, Bosch P, Rivarola CR, Cytotoxicity and bioadhesive properties of poly-N-isopropylacrylamide hydrogel, Heliyon. 5 (2019) e01474. [PubMed: 31008402]

[28]. Scherzinger C, Schwarz A, Bardow A, Leonhard K, Richtering W, Cononsolvency of poly-N-isopropyl acrylamide (PNIPAM): Microgels versus linear chains and macrogels, Current opinion in colloid & interface science. 19 (2014) 84–94.

[29]. Podewitz M, Wang Y, Quoika PK, Loeffler JR, Schauperl M, Liedl KR, Coil–Globule Transition Thermodynamics of Poly (N-isopropylacrylamide), The Journal of Physical Chemistry B. 123 (2019) 8838–8847. [PubMed: 31545046]

[30]. Tavagnacco L, Zaccarelli E, Chiessi E, On the molecular origin of the cooperative coil-to-globule transition of poly (N-isopropylacrylamide) in water, Physical Chemistry Chemical Physics. 20 (2018) 9997–10010. [PubMed: 29619464]

[31]. Liaw C, Ji S, Guvendiren M, Engineering 3D hydrogels for personalized in vitro human tissue models, Advanced healthcare materials. 7 (2018) 1701165.

[32]. Gan T, Guan Y, Zhang Y, Thermogelable PNIPAM microgel dispersion as 3D cell scaffold: effect of syneresis, Journal of Materials Chemistry. 20 (2010) 5937–5944.

[33]. Wang D, Cheng D, Guan Y, Zhang Y, Thermoreversible hydrogel for in situ generation and release of HepG2 spheroids, Biomacromolecules. 12 (2011) 578–584. [PubMed: 21247096]

[34]. Wei W, Hu X, Qi X, Yu H, Liu Y, Li J, Zhang J, Dong W, A novel thermo-responsive hydrogel based on salecan and poly (N-isopropylacrylamide): Synthesis and characterization, Colloids and Surfaces B: Biointerfaces. 125 (2015) 1–11. [PubMed: 25460596]

[35]. Edmondson R, Broglie JJ, Adcock AF, Yang L, Three-dimensional cell culture systems and their applications in drug discovery and cell-based biosensors, Assay and drug development technologies. 12 (2014) 207–218. [PubMed: 24831787]

[36]. Zuchowska A, Jastrzebska E, Zukowski K, Chudy M, Dybko A, Brzozka Z, A549 and MRC-5 cell aggregation in a microfluidic Lab-on-a-chip system, Biomicrofluidics. 11 (2017) 024110. [PubMed: 28405259]

[37]. Monteiro MV, Gaspar VM, Ferreira LP, Mano JF, Hydrogel 3D in vitro tumor models for screening cell aggregation mediated drug response, Biomaterials Science. 8 (2020) 1855–1864. [PubMed: 32091033]

[38]. Graat H, Witlox MA, Schagen F, Kaspers G, Helder MN, Bras J, Schaap GR, Gerritsen WR, Wuisman P, Van Beusechem VW, Different susceptibility of osteosarcoma cell lines and primary cells to treatment with oncolytic adenovirus and doxorubicin or cisplatin, Br. J. Cancer 94 (2006) 1837–1844. [PubMed: 16736005]

[39]. Lamego I, Duarte IF, Marques MPM, Gil AM, Metabolic markers of MG-63 osteosarcoma cell line response to doxorubicin and methotrexate treatment: comparison to cisplatin, Journal of proteome research. 13 (2014) 6033–6045. [PubMed: 25382592]

[40]. Lin SW, Li XQ, Liu SY, Shi JM, Xu JH, Mao LH, Yin M, Inhibition of Combination of Icaritin and Doxorubicin on Human Osteosarcoma MG-63 Cells in vitro, Zhongguo Zhong xi yi jie he za zhi Zhongguo Zhongxiyi jiehe zazhi= Chinese journal of integrated traditional and Western medicine. 36 (2016) 729–734. [PubMed: 27491234]

[41]. Ouyang Z, Li X, Inhibitory effects of tamoxifen and doxorubicin, alone and in combination, on the proliferation of the MG63 human osteosarcoma cell line, Oncology letters. 6 (2013) 970–976. [PubMed: 24137447]

[42]. Curran S, Achilli T, Leary E, Wilks BT, Vantangoli MM, Boekelheide K, Morgan JR, A 3D spheroid system to evaluate inhibitors of the ABCG2 transporter in drug uptake and penetration, Technology. 3 (2015) 54–63.

[43]. Fukuda J, Khademhosseini A, Yeo Y, Yang X, Yeh J, Eng G, Blumling J, Wang C, Kohane DS, Langer R, Micromolding of photocrosslinkable chitosan hydrogel for spheroid microarray and co-cultures, Biomaterials. 27 (2006) 5259–5267. [PubMed: 16814859]

[44]. Dini S, Binder BJ, Fischer SC, Mattheyer C, Schmitz A, Stelzer E, Bean NG, Green J, Identifying the necrotic zone boundary in tumour spheroids with pair-correlation functions, Journal of The Royal Society Interface. 13 (2016) 20160649.

[45]. Kasinskas RW, Venkatasubramanian R, Forbes NS, Rapid uptake of glucose and lactate, and not hypoxia, induces apoptosis in three-dimensional tumor tissue culture, Integrative Biology. 6 (2014) 399–410. [PubMed: 24503640]

[46]. Luo Y, Hossain M, Wang C, Qiao Y, Ma L, Su M, On-chip radiation biodosimetry with three-dimensional microtissues, Analyst. 137 (2012) 3441–3444. [PubMed: 22701873]

[47]. Thakuri PS, Liu C, Luker GD, Tavana H, Biomaterialsâ€• Based Approaches to Tumor Spheroid and Organoid Modeling, Advanced healthcare materials. 7 (2018) 1700980.

[48]. Gong X, Lin C, Cheng J, Su J, Zhao H, Liu T, Wen X, Zhao P, Generation of multicellular tumor spheroids with microwell-based agarose scaffolds for drug testing, PloS one. 10 (2015)e0130348. [PubMed: 26090664]

[49]. Baek N, Seo OW, Kim M, Hulme J, An SSA, Monitoring the effects of doxorubicin on 3D-spheroid tumor cells in real-time, OncoTargets and therapy. 9 (2016) 7207. [PubMed: 27920558]

[50]. Nash ME, Carroll WM, Nikoloskya N, Yang R, Connell CO, Gorelov AV, Dockery P, Liptrot C, Lyng FM, Garcia A, Straightforward, one-step fabrication of ultrathin thermoresponsive films from commercially available pNIPAm for cell culture and recovery, ACS applied materials & interfaces. 3 (2011) 1980–1990. [PubMed: 21534571]

[51]. Elloumiâ€• Hannachi I, Yamato M, Okano T, Cell sheet engineering: a unique nanotechnology for scaffoldaâ€• free tissue reconstruction with clinical applications in regenerative medicine, J. Intern. Med 267 (2010) 54–70. [PubMed: 20059644]

[52]. Zanoni M, Piccinini F, Arienti C, Zamagni A, Santi S, Polico R, Bevilacqua A, Tesei A, 3D tumor spheroid models for in vitro therapeutic screening: a systematic approach to enhance the biological relevance of data obtained, Scientific reports. 6 (2016) 1–11. [PubMed: 28442746]

[53]. Mehta G, Hsiao AY, Ingram M, Luker GD, Takayama S, Opportunities and challenges for use of tumor spheroids as models to test drug delivery and efficacy, J. Controlled Release. 164 (2012) 192–204.

[54]. Lazzari G, Couvreur P, Mura S, Multicellular tumor spheroids: a relevant 3D model for the in vitro preclinical investigation of polymer nanomedicines, Polymer Chemistry. 8 (2017) 4947–4969.

[55]. Mizutani A, Kikuchi A, Yamato M, Kanazawa H, Okano T, Preparation of thermoresponsive polymer brush surfaces and their interaction with cells, Biomaterials. 29 (2008) 2073–2081. [PubMed: 18261791]

[56]. Li L, Zhu Y, Li B, Gao C, Fabrication of thermoresponsive polymer gradients for study of cell adhesion and detachment, Langmuir. 24 (2008) 13632–13639. [PubMed: 18980353]

[57]. Conzatti G, Ayadi F, Cavalie S, Carrere N, Tourrette A, Thermosensitive PNIPAM grafted alginate/chitosan PEC, Appl. Surf. Sci 467 (2019) 940–948.

[58]. Wang T, Liu D, Lian C, Zheng S, Liu X, Tong Z, Large deformation behavior and effective network chain density of swollen poly (N-isopropylacrylamide)â€“laponite nanocomposite hydrogels, Soft Matter. 8 (2012) 774–783.

[59]. Lei KF, Ji W, Goh A, Huang C, Lee M, Investigation of uniform sized multicellular spheroids raised by microwell arrays after the combined treatment of electric field and anti-cancer drug, Biomed. Microdevices 21 (2019) 94. [PubMed: 31686216]

[60]. Barros AS, Costa EC, Nunes AS, de Melo-Diogo D, Correia IJ, Comparative study of the therapeutic effect of Doxorubicin and Resveratrol combination on 2D and 3D (spheroids) cell culture models, Int. J. Pharm 551 (2018) 76–83. [PubMed: 30217766]

[61]. Eilenberger C, Rothbauer M, Ehmoser E, Ertl P, Küpcü S, Effect of spheroidal age on sorafenib diffusivity and toxicity in a 3D HepG2 spheroid model, Scientific reports. 9 (2019) 1–11. [PubMed: 30626917]

[62]. Dhamecha D, Le D, Movsas R, Gonsalves A, Menon JU, Porous polymeric microspheres with controllable pore diameters for tissue engineered lung tumor model development, Frontiers in bioengineering and biotechnology. 8 (2020) 799. [PubMed: 32754585]

[63]. Sambale F, Lavrentieva A, Stahl F, Blume C, Stiesch M, Kasper C, Bahnemann D, Scheper T, Three dimensional spheroid cell culture for nanoparticle safety testing, J. Biotechnol 205 (2015) 120–129. [PubMed: 25595712]

[64]. Conte C, Mastrotto F, Taresco V, Tchoryk A, Quaglia F, Stolnik S, Alexander C, Enhanced uptake in 2D-and 3D-lung cancer cell models of redox responsive PEGylated nanoparticles with sensitivity to reducing extra-and intracellular environments, J. Controlled Release. 277 (2018) 126–141.

[65]. Liu J, Abate W, Xu J, Corry D, Kaul B, Jackson SK, Three-dimensional spheroid cultures of A549 and HepG2 cells exhibit different lipopolysaccharide (LPS) receptor expression and LPS-induced cytokine response compared with monolayer cultures, Innate immunity. 17 (2011)245–255. [PubMed: 20418262]

[66]. Bell CC, Dankers AC, Lauschke VM, Sison-Young R, Jenkins R, Rowe C, Goldring CE, Park K, Regan SL, Walker T, Comparison of hepatic 2D sandwich cultures and 3D spheroids for long-term toxicity applications: a multicenter study, Toxicological Sciences. 162 (2018) 655–666. [PubMed: 29329425]

[67]. Thoms S, Ali AI, Jonczyk R, Scheper T, Blume C, Tacrolimus inhibits angiogenesis and induces disaggregation of endothelial cells in spheroids—toxicity testing in a 3D cell culture approach, Toxicology in Vitro. 53 (2018) 10–19. [PubMed: 30048735]

[68]. Sahai E, Astsaturov I, Cukierman E, DeNardo DG, Egeblad M, Evans RM, Fearon D, Greten FR, Hingorani SR, Hunter T, A framework for advancing our understanding of cancer-associated fibroblasts, Nature Reviews Cancer. 20 (2020) 174–186. [PubMed: 31980749]

[69]. Nashimoto Y, Okada R, Hanada S, Arima Y, Nishiyama K, Miura T, Yokokawa R, Vascularized cancer on a chip: The effect of perfusion on growth and drug delivery of tumor spheroid, Biomaterials. 229 (2020) 119547. [PubMed: 31710953]

[70]. Tan Y, Suarez A, Garza M, Khan AA, Elisseeff J, Coon D, Human fibroblastmacrophage tissue spheroids demonstrate ratio-dependent fibrotic activity for in vitro fibrogenesis model development, Biomaterials science. 8 (2020) 1951–1960. [PubMed: 32057054]

[71]. Santini MT, Rainaldi G, Romano R, Ferrante A, Clemente S, Motta A, Indovina PL, MG- 63 human osteosarcoma cells grown in monolayer and as three- dimensional tumor spheroids present a different metabolic profile: a 1H NMR study, FEBS Lett. 557 (2004) 148–154. [PubMed: 14741358]

[72]. Santo VE, Estrada MF, Rebelo SP, Abreu S, Silva I, Pinto C, Veloso SC, Serra AT, Boghaert E, Alves PM, Adaptable stirred-tank culture strategies for large scale production of multicellular spheroid-based tumor cell models, J. Biotechnol 221 (2016) 118–129. [PubMed: 26815388]

[73]. Kessel S, Cribbes S, Bonasu S, Rice W, Qiu J, Chan LL, Real- time viability and apoptosis kinetic detection method of 3D multicellular tumor spheroids using the Celigo Image Cytometer, Cytometry Part A. 91 (2017) 883–892.

[74]. Sambale F, Lavrentieva A, Stahl F, Blume C, Stiesch M, Kasper C, Bahnemann D, Scheper T, Three dimensional spheroid cell culture for nanoparticle safety testing, J. Biotechnol 205 (2015) 120–129. [PubMed: 25595712]

[75]. Song Y, Ye M, Zhou J, Wang Z, Zhu X, Restoring E-cadherin expression by natural compounds for anticancer therapies in genital and urinary cancers, Molecular Therapy-Oncolytics. 14 (2019) 130–138. [PubMed: 31194121]

[76]. Yang J, Weinberg RA, Epithelial-mesenchymal transition: at the crossroads of development and tumor metastasis, Developmental cell. 14 (2008) 818–829. [PubMed: 18539112]

[77]. Huber MA, Kraut N, Beug H, Molecular requirements for epithelialâ€“mesenchymal transition during tumor progression, Curr. Opin. Cell Biol 17 (2005) 548–558. [PubMed: 16098727]

[78]. Semenza GL, Hypoxia, clonal selection, and the role of HIF-1 in tumor progression, Crit. Rev. Biochem. Mol. Biol 35 (2000) 71–103. [PubMed: 10821478]

[79]. Muz B, de la Puente P, Azab F, Azab AK, The role of hypoxia in cancer progression, angiogenesis, metastasis, and resistance to therapy, Hypoxia. 3 (2015) 83. [PubMed: 27774485]

[80]. Vaupel P, Harrison L, Tumor hypoxia: causative factors, compensatory mechanisms, and cellular response, Oncologist. 9 (2004) 4–9.

[81]. Liao D, Johnson RS, Hypoxia: a key regulator of angiogenesis in cancer, Cancer Metastasis Rev. 26 (2007) 281–290. [PubMed: 17603752]

[82]. Mak P, Leav I, Pursell B, Bae D, Yang X, Taglienti CA, Gouvin LM, Sharma VM, Mercurio AM, ER² impedes prostate cancer EMT by destabilizing HIF-1α and inhibiting VEGF-mediated snail nuclear localization: implications for Gleason grading, Cancer cell. 17 (2010)319–332. [PubMed: 20385358]

[83]. Krishnamachary B, Semenza GL, Analysis of Hypoxia- Inducible Factor 1α Expression and its Effects on Invasion and Metastasis, Meth. Enzymol 435 (2007) 347–354.

[84]. Erler JT, Bennewith KL, Nicolau M, Domhöfer N, Kong C, Le Q, Chi JA, Jeffrey SS, Giaccia AJ, Lysyl oxidase is essential for hypoxia-induced metastasis, Nature. 440 (2006) 1222–1226. [PubMed: 16642001]

[85]. Crabtree HG, Cramer W, The action of radium on cancer cells. II.—Some factors determining the susceptibility of cancer cells to radium, Proceedings of the Royal Society of London. Series B, Containing Papers of a Biological Character. 113 (1933) 238–250.

[86]. Hockel M, Vaupel P, Tumor hypoxia: definitions and current clinical, biologic, and molecular aspects, J. Natl. Cancer Inst 93 (2001) 266–276. [PubMed: 11181773]

[87]. Minchinton AI, Tannock IF, Drug penetration in solid tumours, Nature Reviews Cancer. 6(2006)583–592. [PubMed: 16862189]

[88]. Grimes DR, Fletcher AG, Partridge M, Oxygen consumption dynamics in steady-state tumour models, Royal Society open science. 1 (2014) 140080. [PubMed: 26064525]

[89]. Sarkar S, Peng C, Kuo CW, Chueh D, Wu H, Liu Y, Chen P, Tung Y, Study of oxygen tension variation within live tumor spheroids using microfluidic devices and multiphoton laser scanning microscopy, RSC advances. 8 (2018) 30320–30329.

[90]. Indovina P, Rainaldi G, Santini MT, Hypoxia increases adhesion and spreading of MG-63 three-dimensional tumor spheroids, Anticancer Res. 28 (2008) 1013–1022. [PubMed: 18507049]

[91]. Roncuzzi L, Pancotti F, Baldini N, Involvement of HIF-1α activation in the doxorubicin resistance of human osteosarcoma cells, Oncol. Rep 32 (2014) 389–394. [PubMed: 24840054]

HIGHLIGHTS

- A thermoresponsive poly N-isopropylacrylamide hydrogel microwell array (PHMA) is reported for high-throughput spheroid generation in a biomimetic environment.
- Cells in the body tend to attach and grow on the extracellular matrix, and will similarly attach to the wells in the PHMA at 37°C.
- Stress-free isolation of cell spheroids can be done using a simple temperature switch.
- Spheroids generated using the PHMA had spherical morphology, developed hypoxia and were used to study cellular responses to doxorubicin.
- This innovative platform can be used for high-throughput spheroid generation and isolation for disease modeling and drug screening applications, in an environment that mimics native cellular milieus.

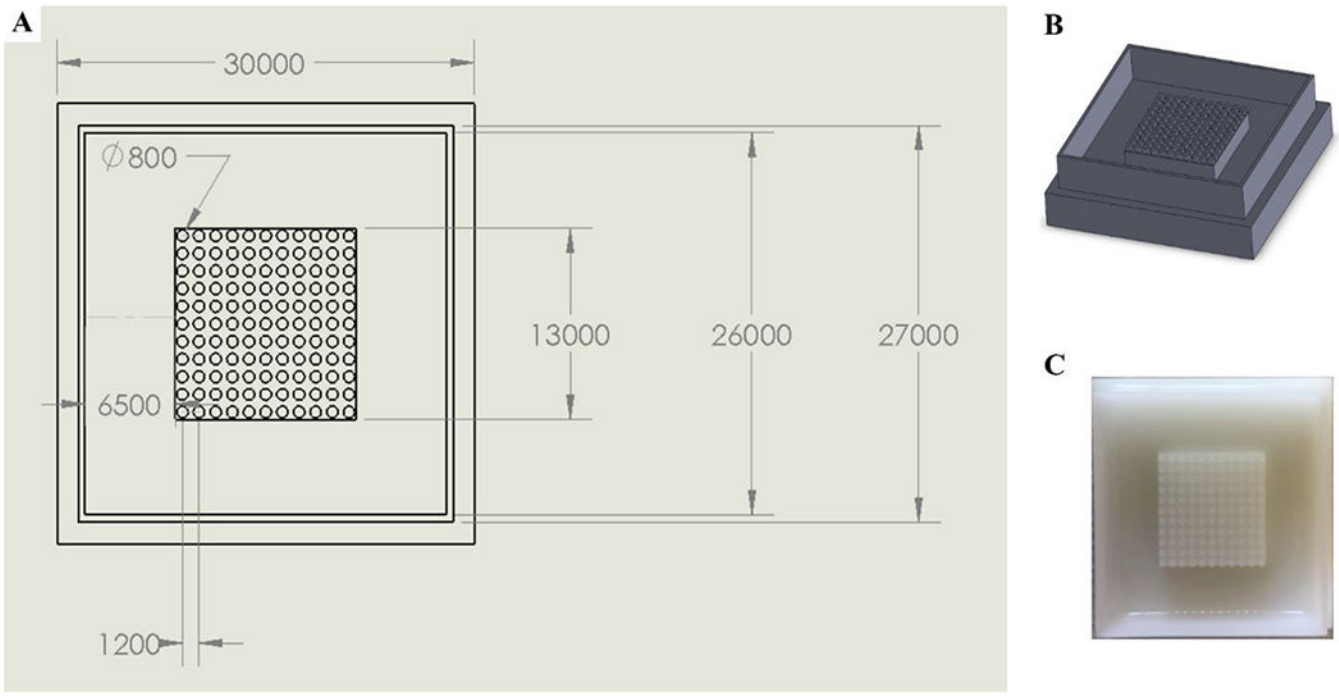

Figure 1:

Design of the negative micromold used to cast the PHMA system, **(A)** Dimensions of the micromold framework, with cylinder diameters of 800 μm. All dimensions are in μm. **(B)** Image of the micromold generated using CAD software. **(C)** Top view of the 3D printed micromold showing cylindrical protrusions on the rectangular framework. These cylinders were used to form the microwells within the PHMA.

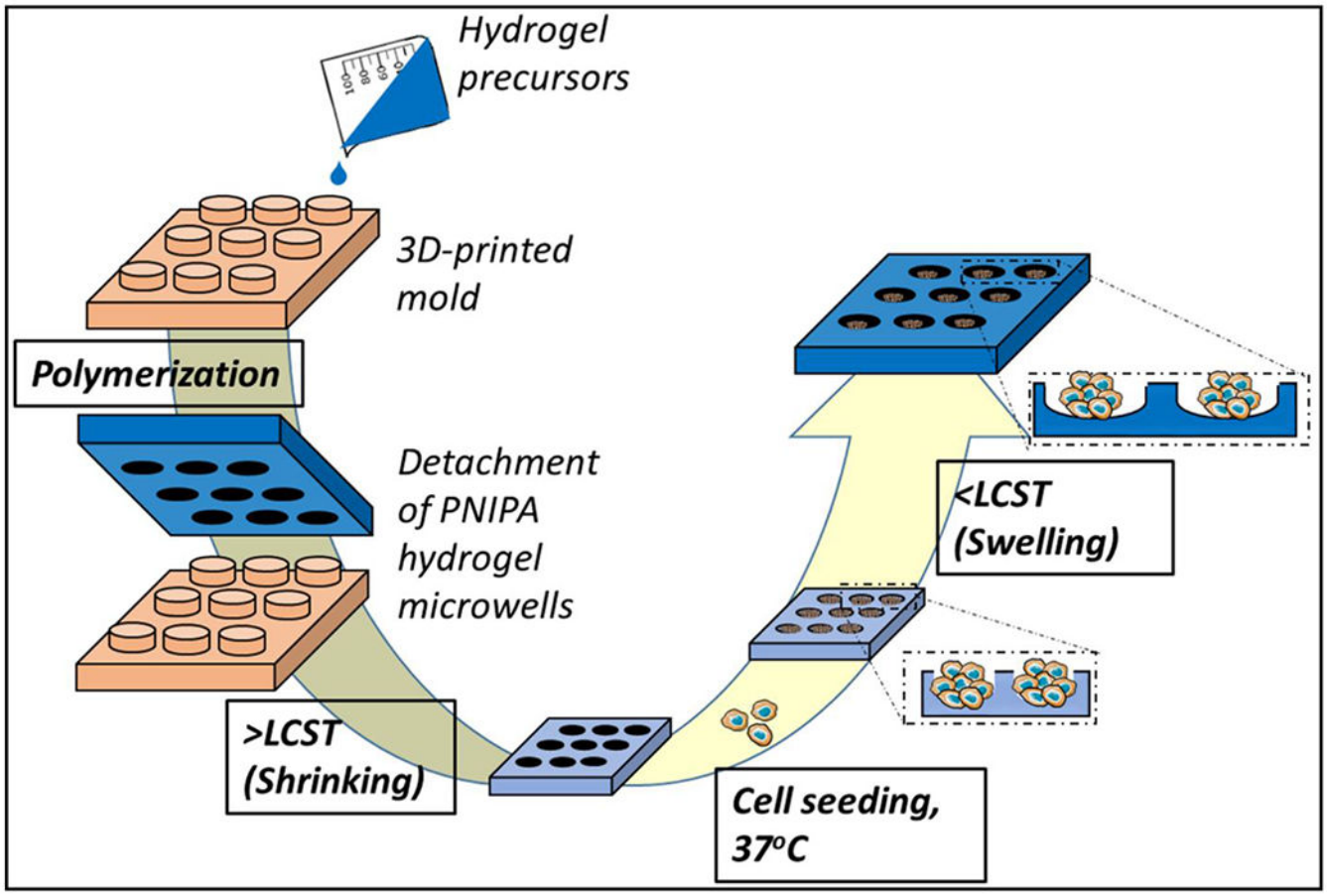

Figure 2:
Schematic representation of fabrication of PHMA, and its application in spheroid generation.

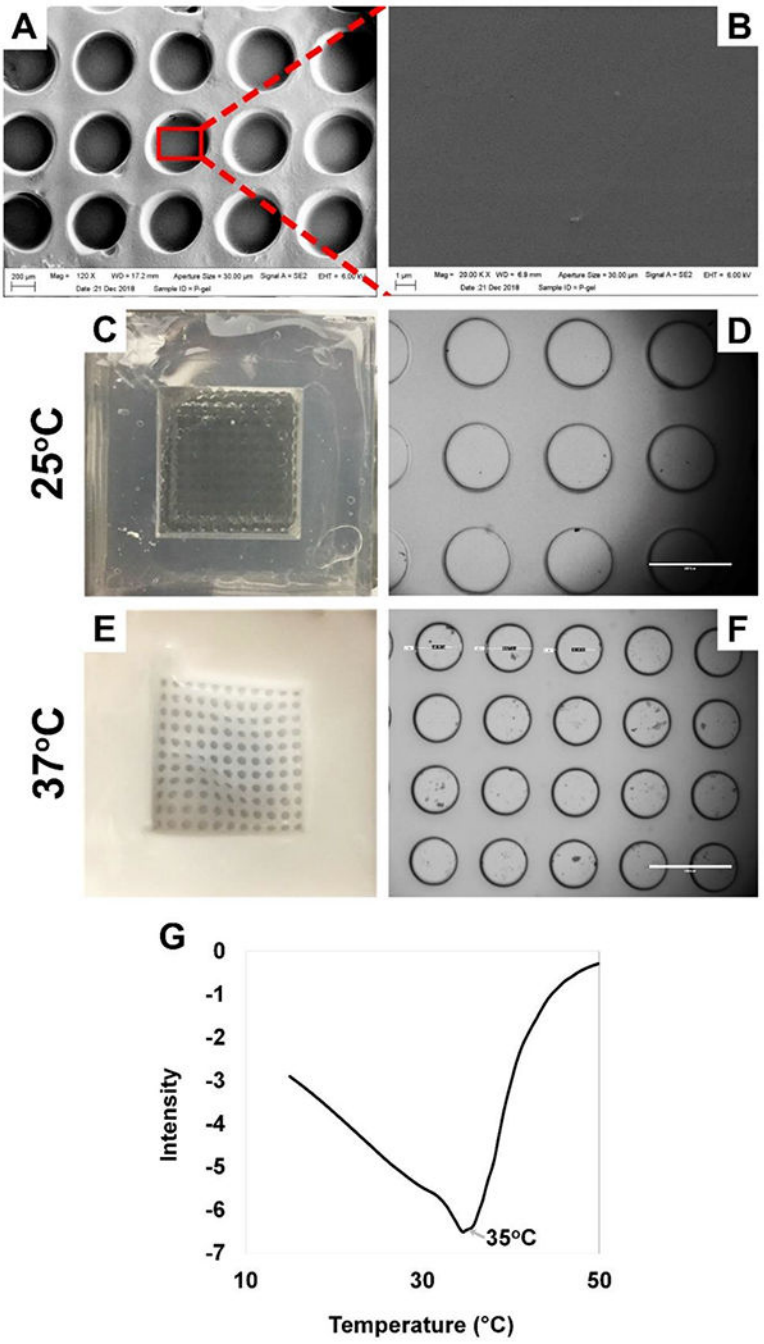

Figure 3:

Characterization of the thermoresponsive behavior of PHMA. SEM image of **(A)** the microwells (Scale = 200 μm) and **(B)** smooth well surface of PHMA (Scale = 1 μm). Representative images of the PHMA at **(C)** 25°C and **(D)** 37°C. EVOS microscope images showing **(E)** swollen wells at 25°C and **(F)** decreased well diameters at 37°C (Scale = 1000 μm). **(G)** DSC thermogram showing thermoresponsive transition of the PNIPAm gel at 35°C.

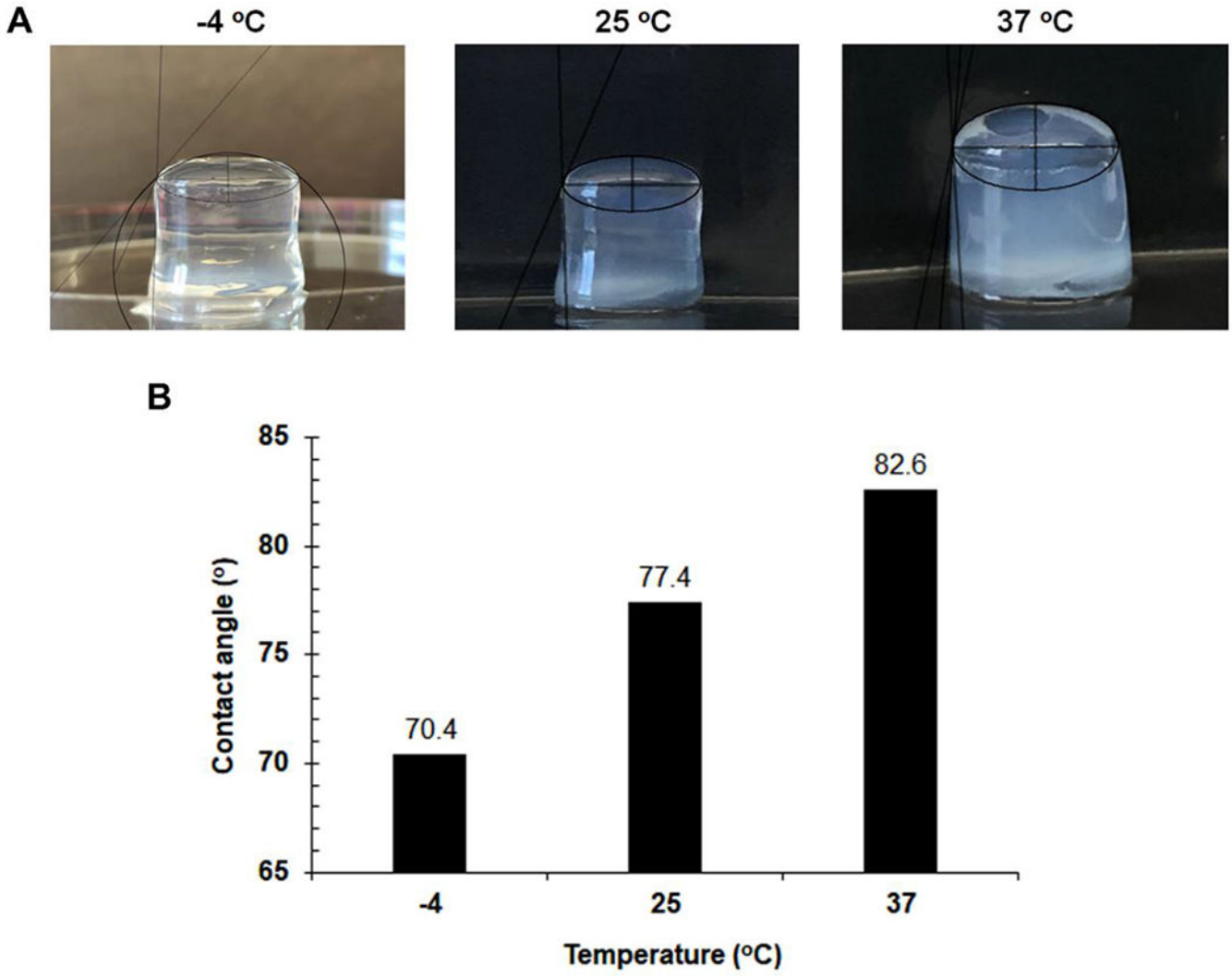

Figure 4:

(A) Representative images and contact angles of the PHMA at different temperatures. **(B)** Quantification of contact angles of PHMA at different temperatures. The same volume of water was added to the surface of each PHMA and the drops were captured on static camera with the same aperture at the same distance. Contact angle was analyzed with multi-point trailing (30 points or more) on border of drops.

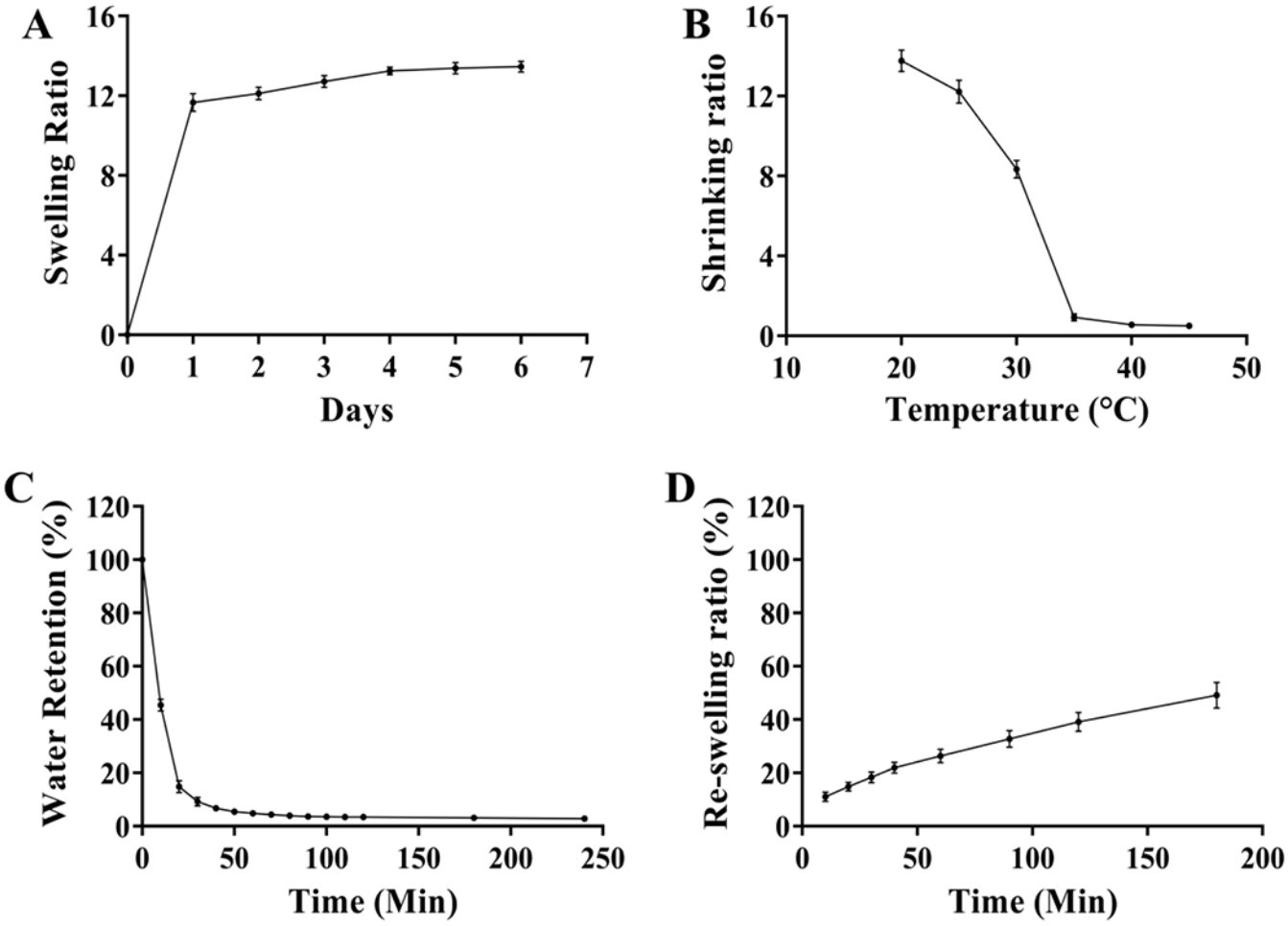

Figure 5:

Characterization of swelling and shrinking properties of PHMA. **(A)** Swelling studies at 25°C show that the PHMA underwent swelling for 24h following which it saturated, **(B)** Maximum shrinking of the hydrogels was observed at ~35°C, **(C)** De-swelling studies at 45°C show that the PHMA underwent maximum shrinking within 50 mins, and **(D)** Re-swelling studies at 25°C shows ~50% swelling within 3 hours (n=3).

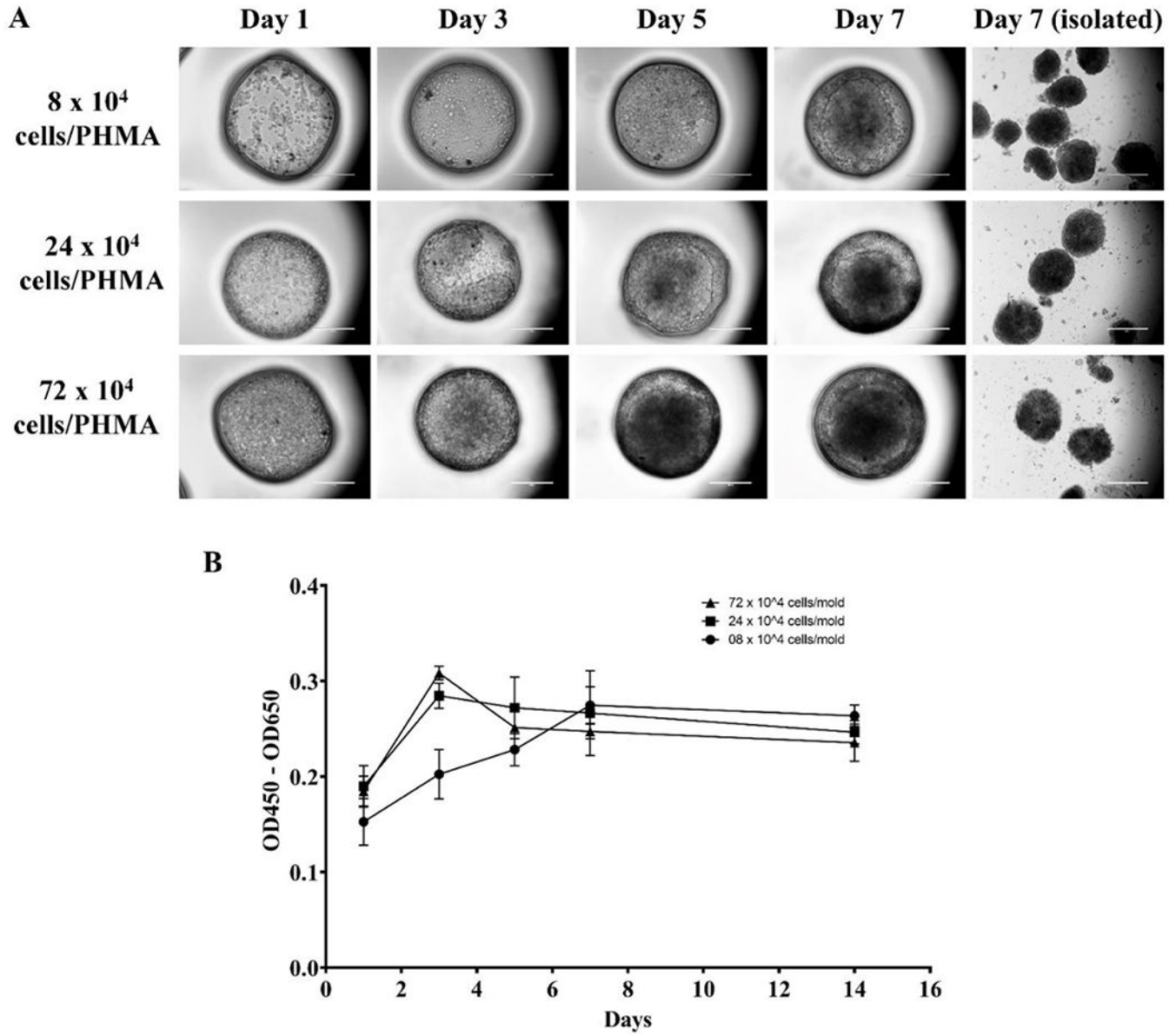

Figure 6:

Cell seeding optimization. **(A)** EVOS brightfield images representing the growth of HeLa cells over time in the PHMA at cell seeding densities of 8×10^4, 24×10^4, 72×10^4 cells/PHMA (scale bar = 400 μm). The last column displays the isolated spheroids on day 7 (scale bar = 200 μm). **(B)** Quantitative analysis of cell viability over time for the different seeding densities was done using WST1 formazan-based assays (n=3).

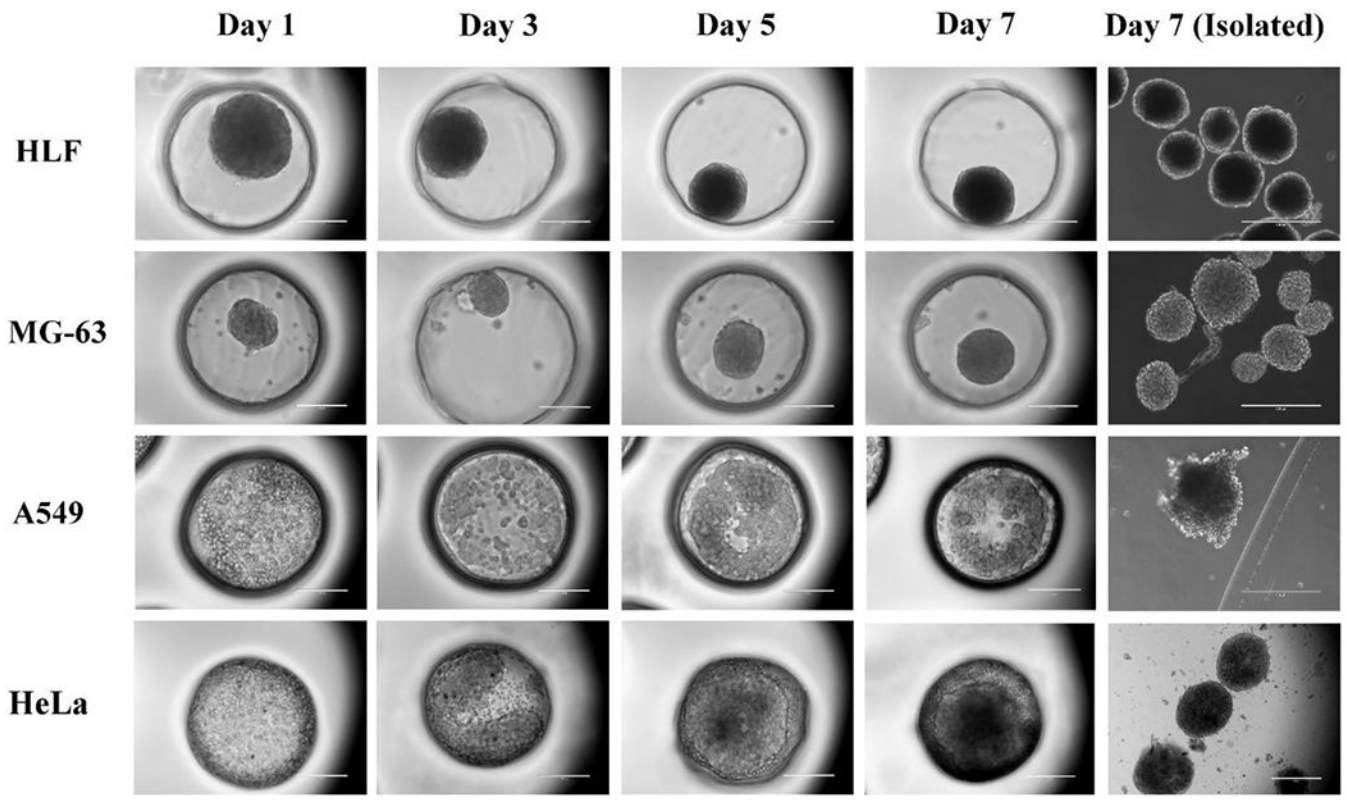

Figure 7:

EVOS brightfield images demonstrating the growth of HLF, MG-63 and A549 spheroids over time in the PHMA. Cell seeding density = 24×10^4 cells/PHMA (scale bar = 200 μm). The last column displays the isolated spheroids on day 7 (scale bar = 400 μm).

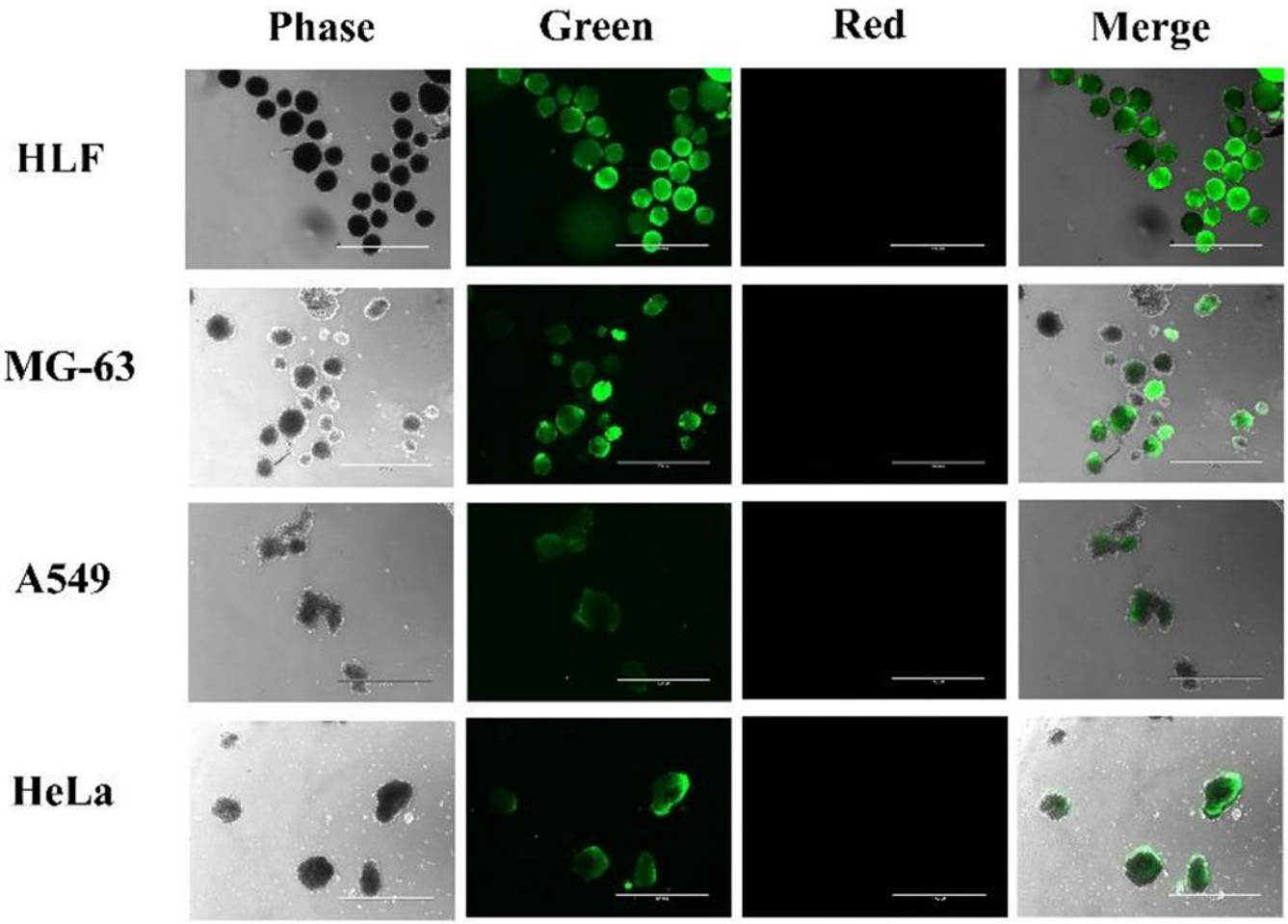

Figure 8:

Fluorescence imaging of HLF, MG-63, A549 and HeLa spheroids at day 7 (scale bar = 1000 μm). Live/dead analysis of spheroids using Calcein AM (green) and ED-1 (red) assay.

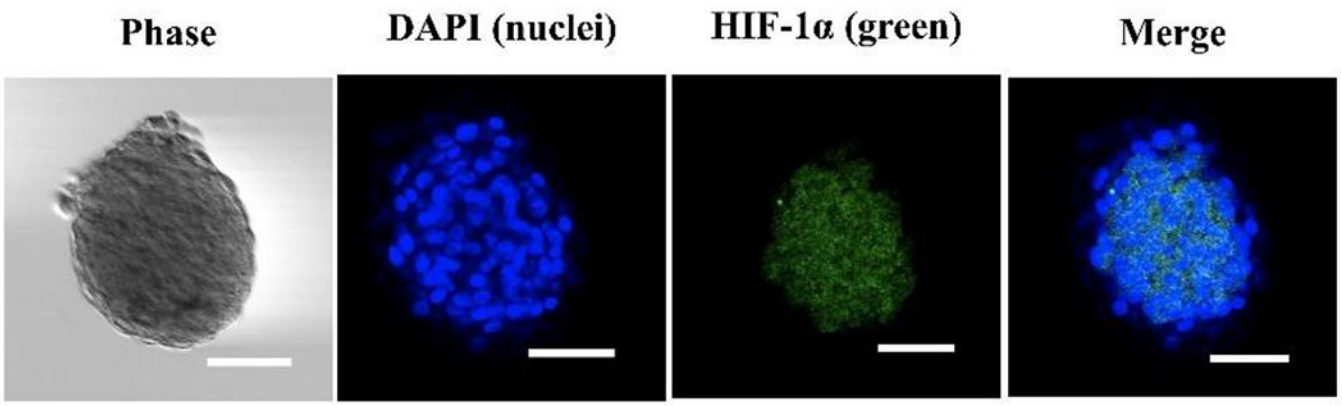

Figure 9:

Immunofluorescence staining of the hypoxia marker HIF1α (green) showing hypoxia within MG-63 spheroids. Spheroids were stained using primary antibody against HIF1α and Alexa Fluor 488 secondary antibody. DAPI was used to stain the nucleus. Images represent a section of the spheroid as captured by Zeiss confocal microscope. (Scale = 100μm).

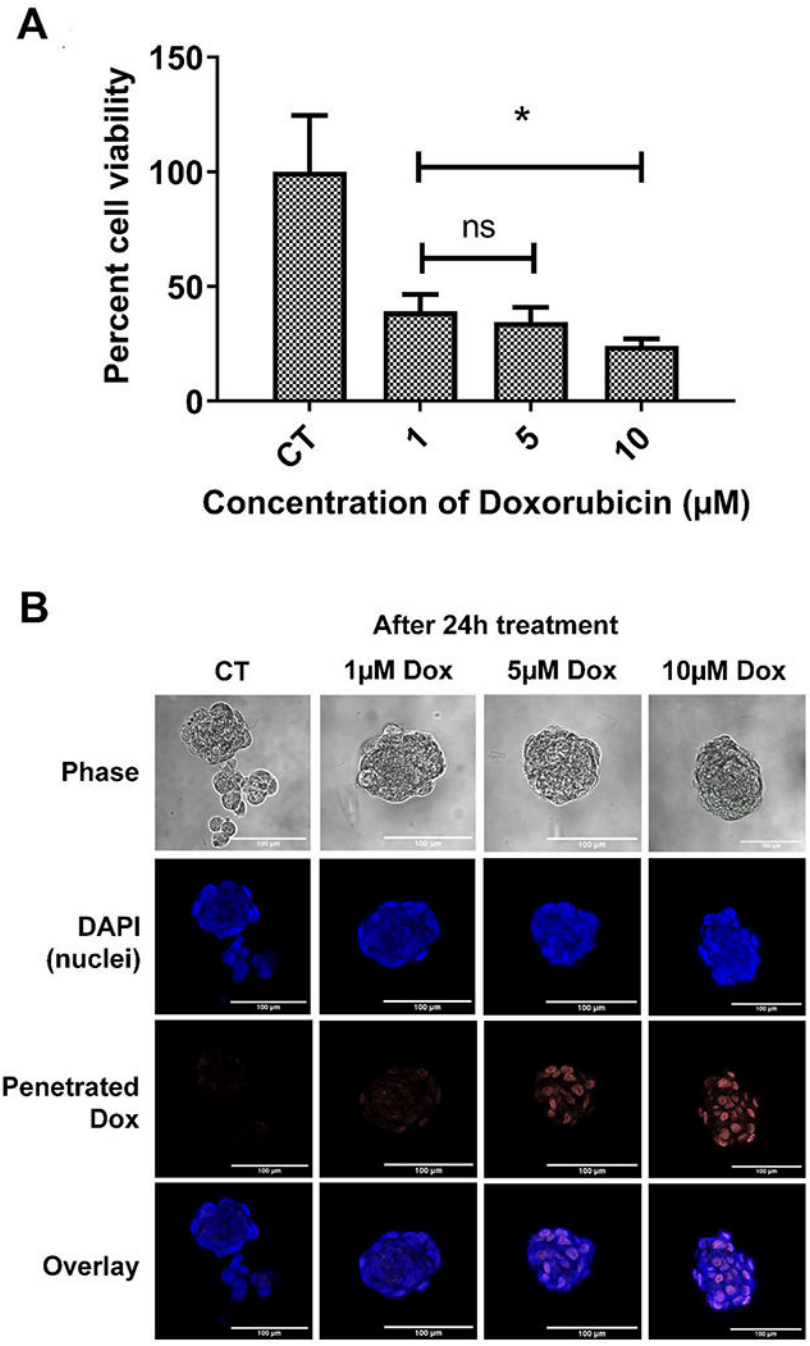

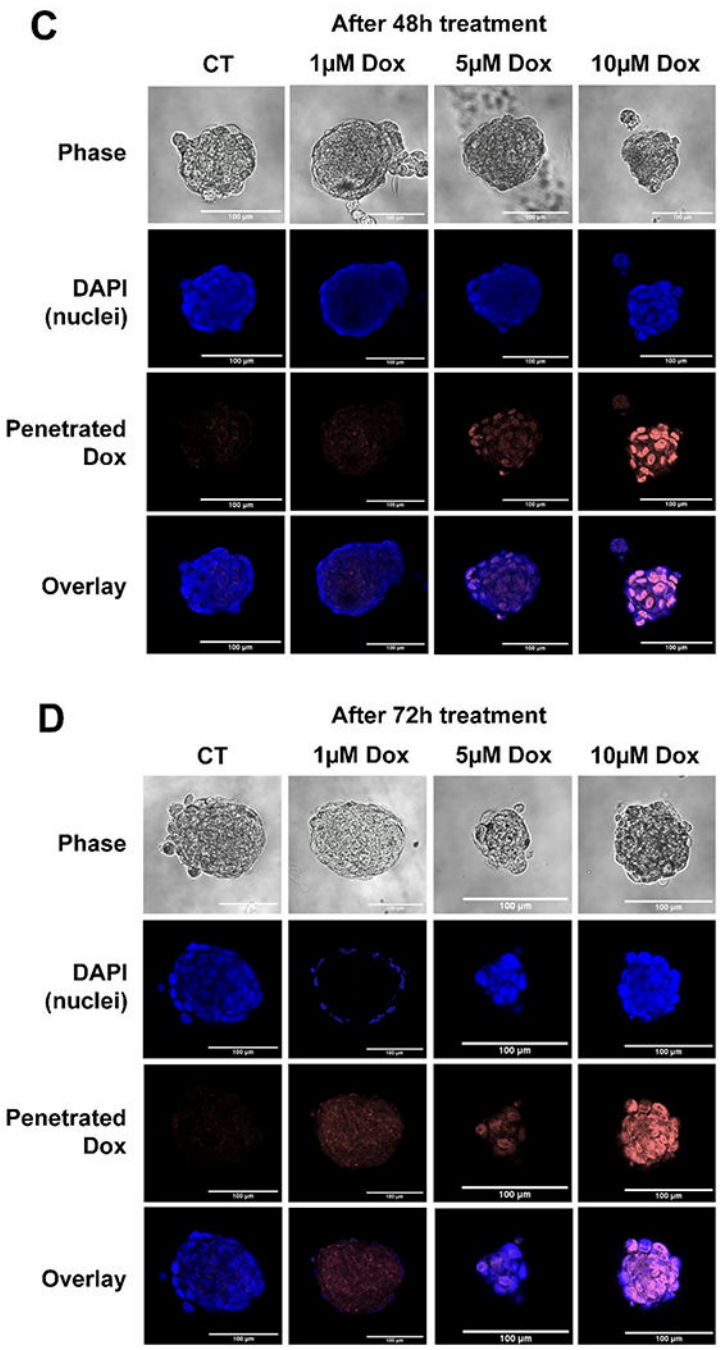

Figure 10:

In vitro drug screening studies. **(A)** Significant decrease in MG-63 spheroid viability observed upon treatment with 10 μM Dox for 72 h; Percent cell viability obtained using Cell Titer Glo assays and calculated as the ratio of luminescence of sample with respect to the untreated control group. *$p<0.01$ using student's t-test. Confocal imaging of spheroids following uptake of Dox (red) at **(B)** 24, **(C)** 48 and **(D)** 72 h of treatment. DAPI (blue) staining of the nuclei was done. Scale bar = 100 μm.